Journal of Materials Chemistry C

ROYAL SOCIETY OF CHEMISTRY

REVIEW

View Article Online
View Journal | View Issue

Cite this: J. Mater. Chem. C, 2022, 10, 2364

Solid additives in organic solar cells: progress and perspectives

Yi-Fan Ma,[a] Yamin Zhang*[a] and Hao-Li Zhang *[ab]

Received 6th September 2021,
Accepted 22nd October 2021

DOI: 10.1039/d1tc04224f

rsc.li/materials-c

The rapid development of organic solar cells (OSCs) has drawn enormous attention during the past few decades. Improving the power conversion efficiency (PCE) is the most important target in the research of OSCs. Active layer morphology plays an essential role in the performance of OSC devices; therefore, great efforts have been made to develop morphology optimization methodologies in order to realize the full potential of photoactive materials. Employing various additives during the fabrication of active layers has been widely used as a very effective method in morphology control. Recently, solid additives have drawn great attention owing to many attractive advantages including good morphology-directing abilities, simple post treatments and enhanced device stabilities. Research has demonstrated that many solid additives can significantly improve the PCE of OSCs, so that they are becoming the key elements for future high-performance OSC devices. However, there is still limited knowledge of the working mechanism of these solid additives, and hence, the general design rules for ideal solid additives are still under development. In this account, we provide a brief overview of the recently reported solid additives, which are categorized into non-volatile and volatile types based on their physical properties. Focused on their basic structures and function mechanisms, both organic and inorganic solid additives are reviewed, which could provide a useful guidance for the design of solid additives. Finally, the challenges and future perspectives of solid additives in OSCs are discussed.

1 Introduction

Photovoltaic (PV) technology provides one of the key green solutions to the exhaustion of fossil energy resources, carbon emission and other energy and ecological problems we are currently facing.[1–3] Organic solar cells, with particular advantages such as semi-transparency, high flexibility, low cost and

[a] State Key Laboratory of Applied Organic Chemistry, Key Laboratory of Special Function Materials and Structure Design, College of Chemistry and Chemical Engineering, Lanzhou University, Lanzhou 730000, P. R. China. E-mail: haoli.zhang@lzu.edu.cn, zym@lzu.edu.cn

[b] Tianjin Key Laboratory of Molecular Optoelectronic Sciences Collaborative Innovation Center of Chemical Science and Engineering, Tianjin 300072, P. R. China

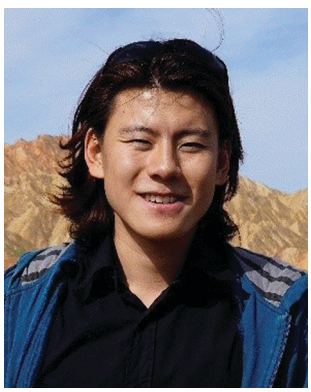

Yi-Fan Ma

Yi-Fan Ma received his BS degree from Dalian University of Technology in 2019. Currently, he is a postgraduate under the supervision of Prof. Hao-Li Zhang at the State Key Laboratory of Applied Organic Chemistry (SKLAOC) of Lanzhou University. His research mainly focuses on the design and synthesis of organic semiconductors and the fabrication of organic solar cells.

Yamin Zhang

Yamin Zhang received her BS degree from Lanzhou University in 2014 and PhD degree from Nankai University in 2019 under the supervision of Prof. Yongsheng Chen and Prof. Xiangjian Wan. In 2019, she joined the State Key Laboratory of Applied Organic Chemistry (SKLAOC) of Lanzhou University as an assistant professor. Her research focuses on the design of small-molecule organic semiconductors and the fabrication of organic functional devices.

large-area printability, have attracted tremendous attention from both academia and industries.[4–6] After thirty years of development, the power conversion efficiency (PCE) of OSC devices has exceeded 18%,[7–13] rapidly approaching that of their inorganic counterparts. The factors that contributed the most to the improvement of PCEs are the innovation of photoactive materials[14–19] and the optimization of the active layer morphologies.[20–22] Bulk-heterojunction (BHJ),[23] as the most commonly used p–n junction in organic solar cells, is composed of at least one couple of donor and acceptor. It is important that the donor and acceptor materials are mixed in an appropriate morphology to allow efficient charge separation and transport. The ideal morphology state requires a suitable crystal domain size (10–20 nm), a bi-continuous interpenetrating network, high phase purity, and reasonable vertical phase separation.[24] However, due to the different crystallization behaviors of the donor and acceptor, it is often difficult to control the active layer morphology and obtain a suitable phase separation that could achieve the best device performance.[25]

In the last decade, a large number of morphology optimization methods have been explored in order to fabricate active layers with ideal morphology and phase separation. Currently, the most commonly used morphology optimization methods can be divided into three categories. (1) Thermal annealing is probably the most traditional and widely used method. Treating the blend film with a period of heating at temperatures around their glass transition temperature could help the molecules rearrange into a state with higher crystalline and phase purity.[26–29] (2) Solvent vapor annealing process treats the blend films in the vapor of certain annealing solvents at room temperature or higher temperatures. During solvent vapor annealing, the different solubilities of the donor and acceptor control their relative motion speed and affect their crystallization behavior. Choosing an appropriate annealing solvent, annealing time and saturated vapor pressure is very important in the optimization process.[30–32] (3) Adding solvent additives is another efficient strategy to achieve ideal morphology. Generally, certain high boiling point (b.p.) solvents or the solvents with selective solubilities for the donor and acceptor in the active layers are employed, which could effectively control the crystallinity and phase separation of the materials.[21] Among them, the addition of solvent additives is one of the most commonly used method to optimize the device morphology. Additives such as 1,8-diiodooctane (DIO),[33,34] octanedithiol (ODT),[35,36] diphenylether (DPE)[37,38] and 1-chloronaphthalene (CN)[39,40] have been demonstrated to be very effective in the manipulation of the phase separation and molecular packing of the corresponding donors or acceptors. However, one problem with these high b.p. solvent additives is that the residual additives will continuously change the morphologies of the active layers, and severely deteriorate the device performances *via* photo-oxidation degradation; thus, the photostability of organic solar cells was dramatically decreased.[41–44] Besides, they are often difficult to be completely removed from the active layer, and the complicated vacuum removal process makes it less fancy in the large-scale fabrication.[45]

Solid additives have been developed recently to avoid the undesirable effects of using solvent additives. The simple post-treatment process and good morphology optimization effect make adding solid additives a reliable optimization method. Moreover, the working mechanisms of solid additives are varied and quite different from the solvent additives. Herein, we review the recent advances of solid additives in OSCs, including material design, performance and mechanism of this morphology optimization method. The solid additives were categorized as non-volatile type and volatile type, and the main difference between them is whether they could be removed from the blend films.[46] The reason for defining the types of solid additives in this way is that some of the additive residues in the active layer will deteriorate the PCE;[47] however, the others need to stay in the active layer to continuously function in the morphology control. Thus, an in-depth understanding of the working mechanisms is of great significance to explore the general design principles of the solid additives.

Hao-Li Zhang

Hao-Li Zhang received his BS and PhD degrees from Lanzhou University, and then worked in the University of Leeds and Oxford University as a postdoc. In 2004, he joined the State Key Laboratory of Applied Organic Chemistry (SKLAOC) of Lanzhou University and became a full professor. Prof. Zhang works on organic semiconductors and nanodevices. He is currently a Fellow of Royal Society of Chemistry (FRSC). He is board member of several academic journals, including Chin. Sci. Bull., Acta Physico-Chimica Sinica, Chin. Chem. Lett. and Chem. Soc. Rev.

2 Non-volatile solid additives

Due to their high boiling point (b.p.), solid additives in this category remained in the blend film after post-treatment. Pyridine derivatives and small molecules that contain hydroxyl groups are the most widely used additives in fullerene organic solar cells. Intermolecular hydrogen bond is believed to be the reason for morphology optimization. Besides, nanomaterials with non-volatile characteristics showed impressive results in performance enhancement of OSCs. Solid additives with excellent optical and electrical properties are quite suitable for the doping of blend films. In view of the wide variety of nanomaterials and their different natures, their function mechanisms are also different.

2.1 Organic small molecules

Many pyridine derivatives and hydroxyl groups containing solid compounds have been investigated in the fullerene-based

OSCs. In 2014, Wu *et al.* came up with the concept of solid additives. They applied a simple non-volatile organic molecule 2,3-dihydroxypyridine (DHP, Fig. 1a), which has a b.p. of 387 °C, into the fullerene-based organic solar cell. The depth profile electron spectroscopy for chemical analysis (ESCA) indicated a reversed vertical composition profile that more P3HT moved toward the anode side, while more $PC_{61}BM$ diffused towards the cathode side. ^{1}H NMR has proved that the additive has a hydrogen bonding with $PC_{61}BM$ *via* the bi-dentate hydroxyl groups. The proposed working mechanism is quite different from commonly used liquid additives. As a result, a dramatic increase in J_{sc} and FF was observed, which led to a higher PCE than the device without solid additives.[51] Later, Xu *et al.* investigated the role of DHP in the P3HT:$IC_{60}BA$ active layer. They claimed that DHP aligned parallel with the side group of $IC_{60}BA$, allowing a full interaction between P3HT and fullerene cage. Enhanced diffraction peak intensities observed in the XRD pattern indicated a more ordered and dense packing of P3HT. The AFM images and water contact angle measurements showed a rich component of $IC_{60}BA$ at the P3HT:$IC_{60}BA$:DHP surface. Such phenomenon was attributed to the differences in the flexibilities of P3HT chains and crystallization behaviors after DHP treatment.[52] Then, they tested the difference between 2-hydroxypyridine (2-HP, Fig. 1a) and 2,4-dihydroxypyridine (2,4-DHP, Fig. 1a). The device of P3HT:$PC_{71}BM$:2-HP exhibits a champion PCE of 4.35% with an improved J_{sc} value of 12.12 mA cm^{-2}.[53] DHP interacts more strongly with the fullerene cage than with the donor material P3HT. However, polymers

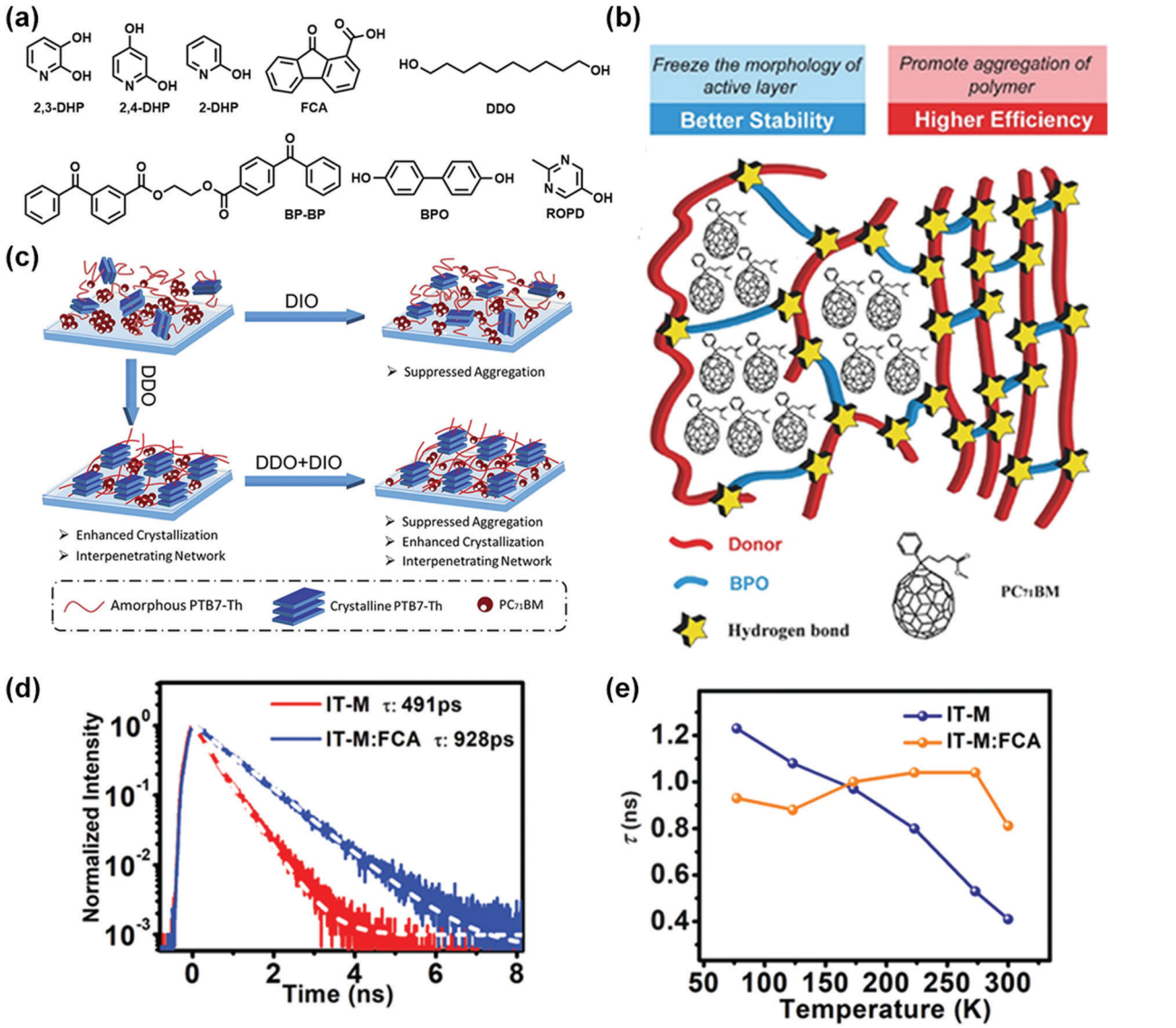

Fig. 1 (a) Chemical structures of non-volatile solid additives. (b) Schematic of the donor, $PC_{71}BM$, BPO, and hydrogen bond in active layers. Reproduced with permission from ref. 50. Copyright 2016, Wiley-VCH. (c) Possible molecular distributions in PTB7-Th:$PC_{71}BM$-based binary films. Reproduced with permission from ref. 49. Copyright 2019, Royal Society of Chemistry. (d) Transient fluorescence spectroscopy of IT-M neat and blend films. (e) Calculated lifetime of singlet excitons in IT-M neat and blend films at 77, 127, 177, 227, 277, and 300 K. Reproduced with permission from ref. 48. Copyright 2020, Wiley-VCH.

with fluorine (F) atoms could form strong H-bonds with hydroxyl groups. A thorough study was conducted by Cheng *et al.* in 2016, and they proposed a concept of "molecular lock" to describe the interaction between solid additive 4,4′-biphenol (BPO, Fig. 1a) and polymer donors that contain F atoms. As shown in Fig. 1b, the strong O–H···F bond promote the π–π stacking of polymer materials and the "lock" can freeze the morphology of blend films. As a result, the F-containing solar cells all had an increase of efficiency after BPO treatment, while the PCEs of active layers without F atoms remained unchanged.[50]

Another organic molecule 5-hydroxy-2-methylpyrimidine (ROPD, Fig. 1a) containing a nitrogen atom and a hydroxyl group was introduced by Zhang *et al.* as a low-cost halogen-free solid additive in PTB7-Th and $PC_{71}BM$ active layers. The device with a ROPD additive exhibited a 13% efficiency improvement compared with the plain device. Hydrogen bond interactions between PTB7-Th/$PC_{71}BM$ and hydroxyl groups in ROPD were proved by Fourier transform infrared (FT-IR) spectra and ^1H NMR spectra. These interactions could lead to more ordered lamellar stacking and interpenetrating network structure of the active layer. Besides, the ROPD containing devices exhibit a higher PCE and a higher stability than those of DIO-containing devices.[54] In order to further improve the device efficiency, adding both solvent and solid additives could be a fascinating strategy. However, successful hybrid additives in solar cells have rarely been reported. Du *et al.* introduced a halogen-free solid additive 1,10-decanediol (DDO, Fig. 1a) into a fullerene-based active layer. The device based on PTB7-Th:$PC_{71}BM$:0.5% DDO exhibits a higher PCE of 10.11% than that of DIO-containing device. Furthermore, they also found that the binary device with 0.5% DDO and 1% DIO added yields the highest PCE of 11.64%. The author proposed that the high boiling point solvent DIO helps to suppress fullerene aggregation, while DDO helps to regulate the polymer donor and enhance crystallization, so that favored charge transportation is achieved (Fig. 1c).[49]

Several additives without hydroxyl groups also function well. Fan *et al.* used a photoinitiator, bifunctional bis-benzophenone, (BP-BP, Fig. 1a) as a non-volatile solid additive. The inverted devices based on the PBDB-T:ITIC system had an increased efficiency from 10.61% to 11.89% after the addition of BP-BP. As suggested by the AFM and GIWAXS measurements, the solid additive can hardly affect the surface morphology of the blend film; however, it can enhance the π–π stacking of polymer donors with a more favored face-on orientation.[55] In addition to modulating the film morphology, another working mechanism of solid additives has been proposed by Guo *et al.* recently. The author investigated the role of a non-volatile solid additive, 9-fluorenone-1-carboxylic acid (FCA, Fig. 1a), in PBDB-T:IT-M BHJ films. By blending FCA with IT-M, stronger photoluminescence and longer exciton lifetime were observed from the emission and transient fluorescence spectroscopies (Fig. 1d), indicating a substantial suppression for non-radiative processes. Besides, the exciton lifetime ranging from 77 to 300 K fluctuates at nearly 950 ps, which is different from the dramatic decrease in the neat IT-M film (Fig. 1e). It was thought that increased rigidity and restricted vibration and torsions of FCA treated IT-M molecules make excitons less fancy non-radiative deactivation path; thus the prolonged lifetime of excitons improved charge transfer and separation. However, a similar phenomenon has not been observed in the PBDB-T and FCA blend.[48]

2.2 Nanomaterials

Nanomaterials have been applied to organic solar cells for several years.[62] Due to their excellent optical and optoelectronic performance,[63–67] they were used as electron transport layer (ETL), hole transport layer (HTL),[68,69] as well as active layer materials in BHJ.[70,71] Bai *et al.* for the first time doped black phosphorus (BP) into PCBM and studied two hybrid heterojunction performance.[71] Lin *et al.* used solution-processed BP as an effective ETL in an inverted solar cell, which has a suitable energy level to form a cascaded band structure with PTB7:$PC_{71}BM$.[68] Wang *et al.* has created sandwiched organic solar cells with two different kinds of black phosphorus quantum dots (BPQDs) coated below and on top of the active layer.[69] Though the nanomaterials are widely used in the field of OSCs, in this review, we only focus on their applications in the BHJ blend films as the solid additives. Carbon-based nanomaterials have attracted the foremost attentions in the OPV field. For instance, Lee *et al.* incorporated Au NP-decorated nitrogen (N)- or boron (B)-doped carbon nanotubes (Au:NCNTs or Au:BCNTs, respectively, Fig. 2a) into OSCs. Both devices resulted in an increased efficiency compared to PTB7:$PC_{70}BM$. The author claimed that using localized surface plasmonic resonance (LSPR) of noble metal nanoparticles (NPs) is a promising way to promote the performance of solar cells. The author found that the PL intensity of PTB7/CNTs is enhanced after the addition of Au NPs, suggesting that the nanomaterial can facilitate excitation and charge dissociation of PTB7. As indicated by GIWAXS analysis, a strong face-on orientation is formed after the addition of Au:CNTs. The Au NPs enhanced the absorption spectra of the blend film from 500 nm to 700 nm, which highly increased the current density of solar cells.[61]

Graphene, as a representative 2D material with high mobility, has been widely applied in photonics and optoelectronics fields.[72] A graphene-based porphyrin molecule (GO-TPP, Fig. 2b) was employed as an electron cascade material in organic solar cells by Stylianakis *et al.*, in which 0.3% of 2D material can lead to a much enhanced current density and FF, resulting in a PCE of 8.58%. They found that the well-matched energy level of GO-TPP acts as an efficient electron-cascade material with photoactive layer materials, improving the performance of solar cells by enhancing the charge transport and reducing exciton recombination between D–A interfaces.[60] Moon *et al.* reported the synthesis and application of N-doped graphitic carbon dots (N-GCDs, Fig. 2c) in photovoltaic devices. They found that 2 wt% of N-GCDs added to PTB7:$PC_{71}BM$ blends leads to 20% enhancement of efficiency. The photoluminescence (PL) decay time of the N-GCDs/$PC_{71}BM$

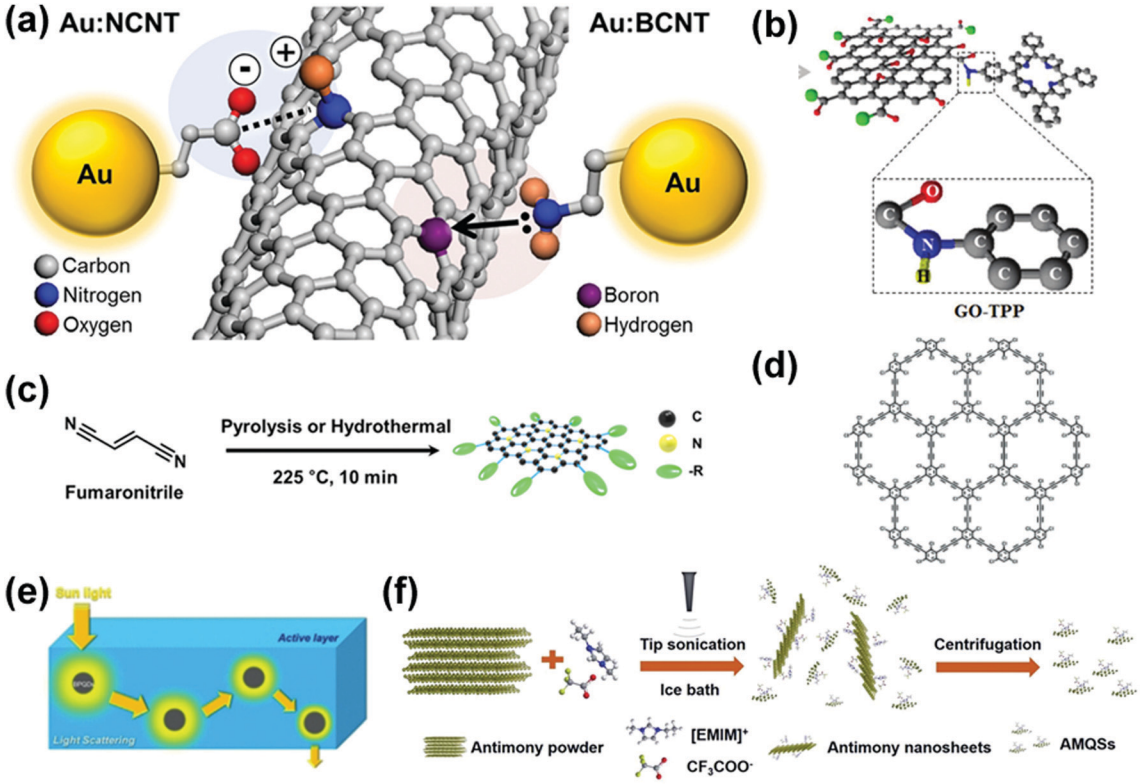

Fig. 2 (a) Schematic of the chemical interactions of Au:NCNT (left) and Au:BCNT (right) hybrids. Reproduced with permission from ref. 61. Copyright 2015, Wiley-VCH. (b) Schematic of the GO-TPP. Reproduced with permission from ref. 60. Copyright 2015, Royal Society of Chemistry. (c) Representation of the Synthesis of N-GCDs using two thermolysis processes. Reproduced with permission from ref. 59. Copyright 2016, American Chemical Society. (d) Chemical structure of GCl Reproduced with permission from ref. 56. Copyright 2020, Wiley-VCH. (e) Schematic diagram of light absorption and scattering by BPQDs in an organic layer. Reproduced with permission from ref. 58. Copyright 2017, Wiley-VCH. (f) Schematic of the fabrication process of AMQSs. Reproduced with permission from ref. 57. Copyright 2018, Royal Society of Chemistry.

blend film (423 ps) is dramatically decreased compared with that of pure N-GCDs (7862 ps), indicating that excitons are well dissociated at N-GCDs/$PC_{71}BM$ interfaces. Besides, there are significant overlap between the absorption spectrum of $PC_{71}BM$ and the PL spectrum of N-GCDs, which facilitated the Förster resonance energy transfer between them.[59] Recently, Liu *et al.* have applied nonvolatile chlorine-functionalized graphdiyne (GCl, Fig. 2d) as a solid additive in PM6:Y6 solar cells and obtained a high PCE of 17.3% compared with the non-added control device (15.6%). Compared with the pure Y6 film, the blend film of Y6:GCl exhibited a red-shifted absorbance, indicating that GCl could act as a nucleation center to promote the crystallization of the acceptor Y6. As a result, the favorable morphology led to a significantly enhanced FF of 79% (Table 1).[56]

Monolayer or few-layered 2D materials of Group 15 (VA) elements (P, As, Sb, and Bi) have recently gained increasing interest, due to their tunable band gap, and electronic and optical properties.[73,74] The energy levels of these VA 2D materials are easily controlled by their sizes. BPQDs were introduced into OSCs by Liu *et al.* Only 0.055 wt% of BPQDs added in the active layer resulted in more than 10% efficiency improvement. The authors claimed that BPQDs with a diameter of 4.5 nm exhibit the highest efficiency of the device, due to its suitable energy level to form a cascaded band structure with the photoactive materials and improve the charge transport efficiency. Besides, the authors reported that BPQDs could induce Rayleigh scattering of light (Fig. 2e), which leads to a higher EQE level and an increased current density. However, by adding BPQDs into the blend film, it has rare effect on carrier transport.[58] Single-layered antimonene, as the same group 2D material with BP, was also used as an additive in OSCs by Wang *et al.* The monolayer β-phase antimonene was exfoliated by sonication in solution (Fig. 2f). The antimonene quantum sheets (AMQSs) with higher stability than black phosphorous were blended into PTB7:$PC_{71}BM$-based inverted solar cells. With a 1.0 mg mL^{-1} concentration of AMQSs added into the blend film, the solar cell exhibited a high J_{sc} of 18.34 mA cm^{-2}, FF of 71.9% and a relative PCE enhancement of 25.6% from 7.76% to 9.75% compared with the control device.[57]

3 Volatile solid additives

Similar to non-volatile additives, volatile solid additives can also function as morphology-directing agents and could be removed after thermal annealing treatment. Volatile solid additives that performed well in OSCs are often the molecules

Table 1 Summary of the photovoltaic parameters of non-volatile solid additives in OSCs

Active layer	Additive	V_{OC}/V	J_{SC}/mA cm^{-2}	FF/%	PCE/%	Ref.
PTB7/$PC_{70}BM$	w/o	0.732	16.71	68.03	8.31	61
	Au:NCNT	0.723	18.21	71.78	9.45	
	Au:BCNT	0.743	18.31	72.09	9.81	
PTB7/$PC_{71}BM$	w/o	0.760	16.27	59.8	7.39	60
	GO-TPP	0.767	17.98	62.1	8.58	
PCDTBT/$PC_{71}BM$	w/o	0.880	11.28	56.7	5.62	
	GO-TPP	0.885	13.38	58.4	6.92	
PTB7/$PC_{71}BM$	w/o	0.73	15.3	65	7.3	59
	N-GCD	0.74	16.6	71	8.6	
PTB7/$PC_{71}BM$	w/o	0.713	16.59	65.1	7.70	58
	BPQD	0.715	18.12	67.2	8.71	
PTB7/$PC_{71}BM$	w/o	0.74	15.72	66.3	7.76	57
	AMQS	0.74	18.34	71.9	9.75	
PM6/Y6	CN	0.844	25.10	73.66	15.61	56
	GCl	0.840	26.09	79.05	17.32	
P3HT/$PC_{61}BM$	w/o	0.60	4.75	52	1.53	51
	2,3-DHP	0.61	10.71	67	4.44	
PTB7/$PC_{71}BM$	w/o	0.728	14.7	68.7	7.42	50
	BPO	0.732	15.2	70.7	8.03	
P3HT:$IC_{60}BA$	w/o	0.83	8.36	63	4.22	52
	2,3-DHP	0.83	9.39	66	5.06	
PTB7-Th:$PC_{71}BM$	w/o	0.778	14.01	53.93	5.88	49
	DDO	0.805	18.07	66.90	10.11	
	DDO/DIO	0.806	19.74	71.30	11.64	
P3HT/$PC_{61}BM$	w/o	0.60	8.52	60	2.89	53
	2-DHP	0.60	12.12	64	4.22	
	2,4-DHP	0.60	9.74	61	3.47	
PBDB-T:IT-M	w/o	0.91	17.72	70.49	11.45	48
	FCA	0.92	18.40	72.65	12.31	
PTB7-Th:$PC_{71}BM$	w/o	0.81	15.15	60.04	7.40	54
	DIO	0.79	14.74	67.23	7.86	
	ROPD	0.80	15.65	66.45	8.33	
PBDB-T:ITIC	w/o	0.872	18.45	65.98	11.17	55
	BP–BP	0.877	19.31	70.28	12.14	

with large dipole moments or highly crystallized structures similar to active layer materials.

Donor–acceptor (D–A)-type small-molecule solid additives were designed for the A–D–A-type photoactive materials, as a similar structure is expected to facilitate the charge transport in the active layers. For example, Yu *et al.* developed a series of volatile solid additives named SA1–SA8. Among them, the compounds exhibited higher volatilization properties resulting in higher device performances. From the UV–Vis spectra, the author found that the solid additives helped to regulate the morphology of acceptors, but rarely affected the polymer donor.

Thermogravimetric analysis implies a volatility temperature of 140 °C. As shown in Fig. 3b and further proved by absorption spectra and FT-IR spectra after thermal annealing (140 °C/10 min), the volatilizable solid additives (from SA-1 to SA-4) were completely removed from the blend film, leaving more space for the further arrangement of acceptor molecules.[46] Then they further investigated the importance of volatilities of solid additives. Both the additives SA-4 and SA-7 (Fig. 3a) can enhance the π–π stacking of the acceptor molecule; however, the non-volatile additive remained in the blend film and resulted in a poor efficiency of 10.3%. On the contrary, the device with the additive completely removed exhibits a highly increased J_{sc} and FF, a slightly decreased V_{oc} and an improved PCE of 13.5%, which is higher than that of the control device (12.1%) (Table 2). The author claimed that the additives with poor volatility are prone to aggregate at the surface of the blend film, which could have a negative effect on the active layer morphology (Fig. 3d).[47] Cai *et al.* reported three fluorinated solid additives (INB-F, Fig. 3a) with 1 to 5 F-atoms on the benzene ring. The volatility of the molecules enhanced along with the increase in the amount of fluorine atoms.

Besides, the strong electronegativity of fluorine atoms leads to the formation of a more positively charged indanone unit, and hence, the INB-5F with most number of F atoms showed the lowest adsorption energy when interacting with the central "D–A–D" part of the acceptor BTP-4F, thus the π–π stacking of acceptor molecules could be further improved. The influence of the interaction between additive molecules and acceptors resulted in a larger acceptor domain size and longer shelf-stability.[75] Similarly, Zhang *et al.* has recently studied the influence of operational lifetime by solid additives. They found that INB-F could decrease the adsorption energy of acceptor molecules; thus, a compact stacking was achieved, leading to an increase in light absorption. Moreover, the INB-F-treated PM6:Y6-BO device showed a T_{80} lifetime (defined as the time over which the efficiency decays to 80% of its initial value) of 523 h, which was greatly improved compared with the solar cell without any additives (66.2 h) and the DIO-treated solar cell (6.6 h). Solvent additives accelerate the burn-in degradation process of the active

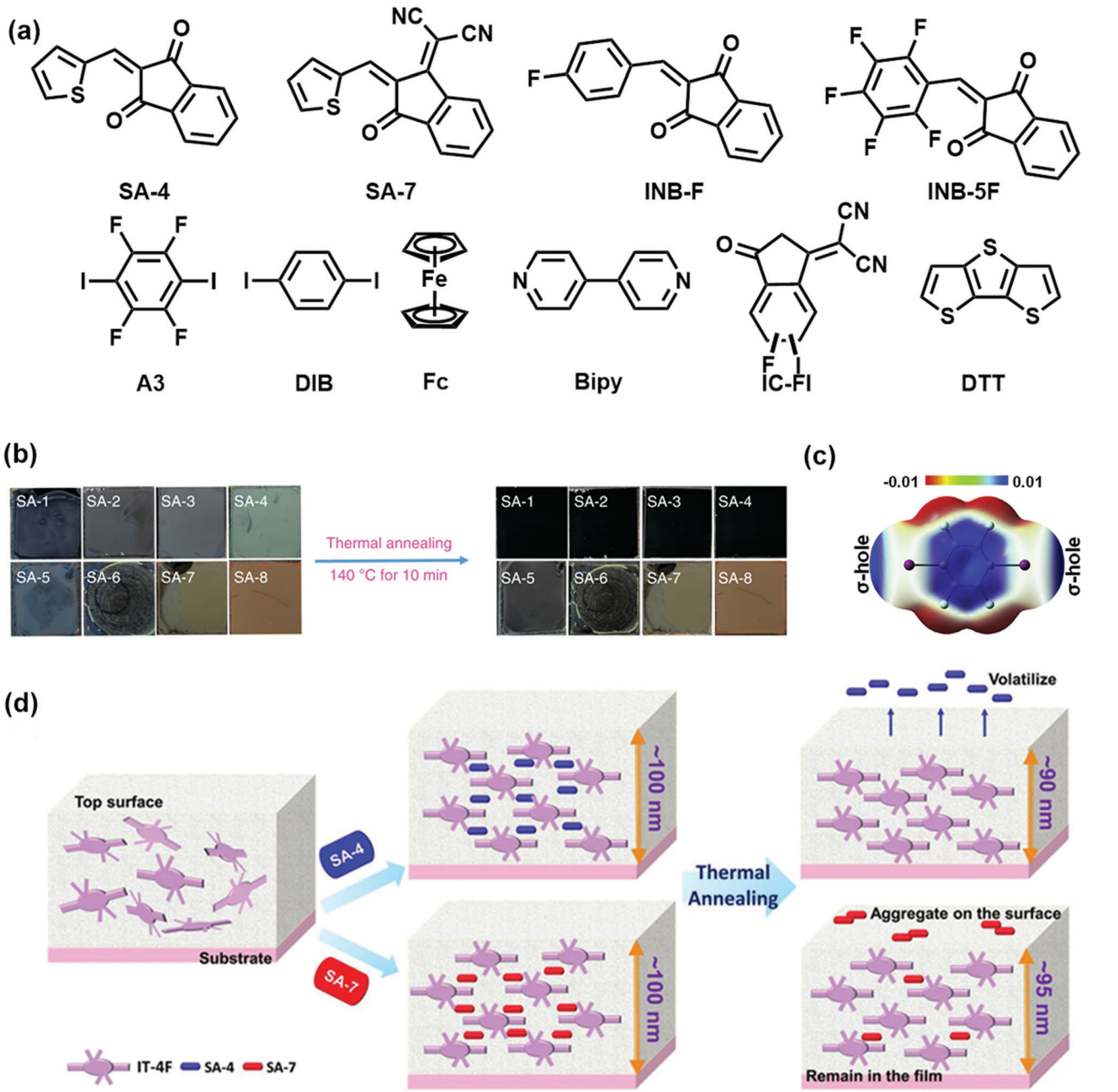

Fig. 3 (a) Chemical structures of volatile solid additives. (b) Photographs of spin-coated films of eight SAs. Then the films were thermal annealed at 140 °C for 10 min. Reproduced with permission from ref. 46.Copyright 2018, Springer Nature. (c) Theoretically simulated electrostatic potential distribution (ESP) of A3 calculated from the density functional theory (DFT) at the BLYP/6–31G level. Reproduced with permission from ref. 77. Copyright 2020, Elsevier. (d) Schematic of the working mechanism of SAs with different volatilities. Reproduced with permission from ref. 47. Copyright 2019, Wiley-VCH.

layers, while the solid additives significantly suppress the process due to their volatility. The results indicated that the solid additive is a promising material in OSC manufacturing as it improves the photostability and PCE[76] It appeared that the D–A-type structure is not essential for small organic additives to have positive effects in OSCs. For instance, a dihalogenated indanone end group IC-FI (Fig. 3a) has achieved a superior PCE in all-small-molecule organic solar cells. IC-FI was easily synthesized, which acted as a volatile solid additive to regulate the morphology. The author demonstrated that the additive slightly reduced the crystallinity of BTR-Cl, which is responsible for the reduced EQE in the range of 300–600 nm. However, the preferred face-on orientation and the more suitable phase separation regulated by IC-FI highly enhanced FF to 73.5%, compared with the control device (64.7%). As a result, the high FF compensates the loss of V_{oc} and J_{sc}, thus a PCE of 14.43% was achieved.[79]

Table 2 Summary of the photovoltaic parameters of volatile solid additives in OSCs

Active layer	Additive	V_{OC}/V	J_{SC}/mA cm^{-2}	FF/%	PCE/%	Ref.
PBDB-TF/IT-4F	w/o	0.89	18.8	71	12.2	46
	SA-1	0.86	20.2	76	13.8	
PBDB-TCl:IT-4F	w/o	0.907	19.0	70.3	12.1	47
	SA-4	0.887	20.4	74.8	13.5	
PBDB-T-2F:BTP-4F	w/o	0.82	26.2	70.1	15.2	75
	INB-5F	0.81	27.1	74.3	16.5	
PM6:Y6-BO	w/o	0.84	26.2	68.8	15.1	76
	INB-F	0.82	26.5	76.7	16.7	
PM6/Y6	w/o	0.86	25.29	68.40	14.8	77
	CN	0.84	25.46	72.90	15.6	
	A3	0.82	26.5	76.05	16.5	
PM6/Y6	w/o	0.838	25.12	72	15.55	78
	CN	0.837	25.90	74	16.50	
	Fc	0.838	26.71	76	17.40	
BTR-Cl/N3	w/o	0.85	24.16	64.7	13.36	79
	IC-FI	0.82	24.06	73.5	14.43	
PM6/Y6	w/o	0.87	24.87	71.13	15.39	80
	DIB	0.84	26.33	78.22	17.36	
J51/N2200	w/o	0.81	15.58	64.37	8.16	81
	Bipy	0.85	14.74	69.44	8.73	

Meanwhile, the mechanisms of several interesting molecules were also investigated. Fu *et al.* introduced a ''σ-hole''-containing volatile solid with an appropriate volatility named A3 (1,4-diiodotetrafluorobenzene, Fig. 3a) in organic solar cells. Density functional theory (DFT) simulation indicates A3 possessed σ-holes, which could form non-covalent interactions with lone electron pairs (for instance, the nitrogen and sulfur atoms in the photoactive materials, Fig. 3c). When A3 was combined with PM6 and Y6 separately, it exhibited a strong vibronic shoulder in the polymer blend film and a slightly redshift of the acceptor film, indicating an enhanced aggregation and ordered packing of the molecules. The high volatility ensures that it can be removed from the blend film completely after thermal annealing at 110 °C for 10 min. The device with A3 showed a slightly decreased V_{oc} but significantly enhanced J_{sc} and FF, thus a PCE of 16.5% was obtained. Furthermore, the efficiencies stayed above 16% when the concentration of additive is varied from 10 mg mL^{-1} to 35 mg mL^{-1}, indicating a high concentration tolerance for practical applications.[77] Another simple halogen atom containing volatile additive 1,4-diiodobenzene (DIB, Fig. 3a) and its performance in OSCs were investigated by Fu *et al.* TGA analysis indicates that DIB could be removed at 110 °C in the TA process. Peaks of DIB in FT-IR spectra disappeared in the TA-treated PM6:Y6:DIB blend film, implying the volatility of DIB. They announced that a eutectic phase was formed between the additive and acceptor molecules, which were proved by differential scanning calorimetry measurement. FT-IR and electrostatic potential surface calculation results indicate that the iodine atom in the DIB molecule interacts with the cyano group of acceptors, assisting the molecular packing and improving the crystalline size. The additive-containing PM6:Y6:ICBA ternary and PM6:Y6 binary device exhibited a PCE of 17.72% and 17.36% respectively.[80] Meanwhile, Ye *et al.* utilized ferrocene (Fc, Fig. 3a) as a highly volatile solid additive in OSCs. This commercially available solid additive could be removed from the blend films at 110 °C for 70 s and demonstrated universal applicability for several different active layers. The increased molecular crystallinity led to an improved charge mobility and suppressed charge recombination. As a result, the efficiency was increased from 15.55% to 17.40% without any loss of V_{oc}.[78]

Inspired by the volatilization property, Yan *et al.* have recently proposed a concept of ''volatile force'' during the evaporation process. They introduced volatile solid additives to all-polymer solar cells for the first time. The additive 4,4′-Bipyridine (Bipy, Fig. 3a) was dissolved with active layers in chloroform and was removed after thermal annealing at 130 °C for 10 min. The author demonstrated that Bipy would interact with polymer acceptor N2200 and enriched the amount of N2200 at the surface during the volatilization process, creating a favorable vertical phase separation. The less donor/acceptor interfaces led to a slightly decreased J_{sc} but a significantly increased V_{oc} and FF, which showed a different function mechanism from other volatile solid additives.[81]

Recently, Bao *et. al.* have demonstrated that volatilizable solid additive dithieno[3,2b:2′,3′-d]thiophene (DTT, Fig. 3a) with high crystallinity could restrict the self-aggregation of acceptor molecules. In addition, a simple treatment of TA at 90 °C for 10 min could completely remove DTT in the blend film. Besides, the combination of CN and DTT could synergistically enhance the J_{sc} and FF of OSCs. As a result, the PTQ10:m-BTP-PhC6:$PC_{71}BM$-based ternary device achieved a remarkable FF of 80.6% and an efficiency of 18.8%, which is the highest in the field.[82]

4 Outlook and conclusions

Although the history of adding solid additives is relatively short, this new strategy has shown many attractive features as soon as it came out. A top PCE of 18.8% has been achieved by the solar cells based on PM6:m-BTP-PhC6:$PC_{71}BM$ with the addition of volatile solid additives and CN. As for non-volatile solid additives, a PCE of 17.32% has also been reached in nanomaterial (GCl)-doped solar cells.[40]

Meanwhile, working mechanisms different from those of solvent additives were explored during the investigation of solid additives. Generally, solid additives could tune the crystallinity of the donor material or acceptor material in the active layer *via* various intermolecular interactions, thereby regulating the phase separation of the active layer, thus improving the performance and stability of the device. It is noteworthy that several hydroxyl groups containing non-volatile organic small molecules showed excellent performance in fullerene-based OSCs. Besides, device performance improvements in non-fullerene organic solar cells were almost all achieved by volatile solid additives. Nanomaterials, yet, show good applicability in both fullerene and non-fullerene systems. A variety of physical properties, excellent stability and solution processability make nanomaterials a promising research part in solid additives. Some of the nanomaterials contribute to the device

performance by producing localized surface plasmonic resonance, assisting charge transfer and inducing Rayleigh scattering of light.

It is notable that non-fullerene acceptor-based organic solar cells have reached the PCE of 18%, which is much higher than that of the devices based on fullerene acceptors. Non-volatile additives and nanomaterials suitable for non-fullerene systems deserve more attention. Moreover, benefiting from their strong electron–electron interactions in the unique electronic structures, as well as the adjustable size,[83,84] these nanomaterials show great potential in OSCs. It is worth noting that some nanoparticles are capable of multiple exciton generation, which might further improve photon utilization.[84,85]

In summary, solid additives have shown great potential in tailoring the active layer morphology and improving the PCE of various OSCs, which greatly broaden the toolbox in photovoltaic research. It is foreseeable that solid additives may play increasingly important roles in the future development of large-scale flexible OSCs.

Conflicts of interest

There are no conflicts to declare.

Acknowledgements

The authors gratefully acknowledge the financial support from National Key R&D Program of China (2017YFA0204903), National Natural Science Foundation of China (NSFC. 51733004, 51525303, 22005128, 21602093), 111 Project, Fundamental Research Funds for the Central Universities and Key Laboratory of Special Function Materials and Structure Design of Ministry of Education (lzujbky-2021-kb06, lzujbky-2020-44).

Notes and references

1 C. J. Brabec, *Sol. Energy Mater. Sol. Cells*, 2004, **83**, 273–292.
2 K. A. Mazzio and C. K. Luscombe, *Chem. Soc. Rev.*, 2015, **44**, 78–90.
3 L. Dou, J. You, Z. Hong, Z. Xu, G. Li, R. A. Street and Y. Yang, *Adv. Mater.*, 2013, **25**, 6642–6671.
4 Q. An, F. Zhang, J. Zhang, W. Tang, Z. Deng and B. Hu, *Energy Environ. Sci.*, 2016, **9**, 281–322.
5 T. Ameri, P. Khoram, J. Min and C. J. Brabec, *Adv. Mater.*, 2013, **25**, 4245–4266.
6 H. Hoppe and N. S. Sariciftci, *J. Mater. Res.*, 2004, **19**, 1924–1945.
7 G. Liu, R. Xia, Q. Huang, K. Zhang, Z. Hu, T. Jia, X. Liu, H.-L. Yip and F. Huang, *Adv. Funct. Mater.*, 2021, **31**, 2103283.
8 L. Meng, Y. Zhang, X. Wan, C. Li, X. Zhang, Y. Wang, X. Ke, Z. Xiao, L. Ding, R. Xia, H.-L. Yip, Y. Cao and Y. Chen, *Science*, 2018, **361**, 1094.
9 J. Qin, L. Zhang, C. Zuo, Z. Xiao, Y. Yuan, S. Yang, F. Hao, M. Cheng, K. Sun, Q. Bao, Z. Bin, Z. Jin and L. Ding, *J. Semicond.*, 2021, **42**, 010501.
10 Q. Liu, Y. Jiang, K. Jin, J. Qin, J. Xu, W. Li, J. Xiong, J. Liu, Z. Xiao, K. Sun, S. Yang, X. Zhang and L. Ding, *Sci. Bull.*, 2020, **65**, 272–275.
11 Y.-N. Chen, M. Li, Y. Wang, J. Wang, M. Zhang, Y. Zhou, J. Yang, Y. Liu, F. Liu, Z. Tang, Q. Bao and Z. Bo, *Angew. Chem., Int. Ed.*, 2020, **59**, 22714–22720.
12 L. Zhan, S. Li, X. Xia, Y. Li, X. Lu, L. Zuo, M. Shi and H. Chen, *Adv. Mater.*, 2021, **33**, 2007231.
13 M. Zhang, L. Zhu, G. Zhou, T. Hao, C. Qiu, Z. Zhao, Q. Hu, B. W. Larson, H. Zhu, Z. Ma, Z. Tang, W. Feng, Y. Zhang, T. P. Russell and F. Liu, *Nat. Commun.*, 2021, **12**, 309.
14 P. Cheng and Y. Yang, *Acc. Chem. Res.*, 2020, **53**, 1218–1228.
15 B. Kan, Y. Kan, L. Zuo, X. Shi and K. Gao, *InfoMat*, 2020, **3**, 175–200.
16 X. Wan, C. Li, M. Zhang and Y. Chen, *Chem. Soc. Rev.*, 2020, **49**, 2828–2842.
17 S. Li, C.-Z. Li, M. Shi and H. Chen, *ACS Energy Lett.*, 2020, **5**, 1554–1567.
18 T. Liu, Y. Zhang, Y. Shao, R. Ma, Z. Luo, Y. Xiao, T. Yang, X. Lu, Z. Yuan, H. Yan, Y. Chen and Y. Li, *Adv. Funct. Mater.*, 2020, **30**, 2000456.
19 R. Zhou, Z. Jiang, Y. Shi, Q. Wu, C. Yang, J. Zhang, K. Lu and Z. Wei, *Adv. Funct. Mater.*, 2020, **30**, 2005426.
20 W. Ma, C. Yang, X. Gong, K. Lee and A. J. Heeger, *Adv. Funct. Mater.*, 2005, **15**, 1617–1622.
21 J. K. Lee, W. L. Ma, C. J. Brabec, J. Yuen, J. S. Moon, J. Y. Kim, K. Lee, G. C. Bazan and A. J. Heeger, *J. Am. Chem. Soc.*, 2008, **130**, 3619–3623.
22 C. Cui and Y. Li, *Aggregate*, 2021, **2**, e31.
23 G. Yu, J. Gao, J. C. Hummelen, F. Wudl and A. J. Heeger, *Science*, 1995, **270**, 1789–1791.
24 M. Pfannmöller, W. Kowalsky and R. R. Schröder, *Energy Environ. Sci.*, 2013, **6**, 2871–2891.
25 G. J. Hedley, A. Ruseckas and I. D. W. Samuel, *Chem. Rev.*, 2017, **117**, 796–837.
26 Y. Kim, S. A. Choulis, J. Nelson, D. D. C. Bradley, S. Cook and J. R. Durrant, *Appl. Phys. Lett.*, 2005, **86**, 063502.
27 I. Constantinou, T.-H. Lai, H.-Y. Hsu, S.-H. Cheung, E. D. Klump, K. S. Schanze, S.-K. So and F. So, *Adv. Electron. Mater.*, 2015, **1**, 1500167.
28 Z. Yi, W. Ni, Q. Zhang, M. Li, B. Kan, X. Wan and Y. Chen, *J. Mater. Chem. C*, 2014, **2**, 7247–7255.
29 E. Verploegen, R. Mondal, C. J. Bettinger, S. Sok, M. F. Toney and Z. Bao, *Adv. Funct. Mater.*, 2010, **20**, 3519–3529.
30 C. Sinturel, M. Vayer, M. Morris and M. A. Hillmyer, *Macromolecules*, 2013, **46**, 5399–5415.
31 S. Miller, G. Fanchini, Y.-Y. Lin, C. Li, C.-W. Chen, W.-F. Su and M. Chhowalla, *J. Mater. Chem.*, 2008, **18**, 306–312.
32 K. C. Dickey, J. E. Anthony and Y. L. Loo, *Adv. Mater.*, 2006, **18**, 1721–1726.
33 J. Kniepert, I. Lange, J. Heidbrink, J. Kurpiers, T. J. K. Brenner, L. J. A. Koster and D. Neher, *J. Phys. Chem. C*, 2015, **119**, 8310–8320.

34 C. Piliego, T. W. Holcombe, J. D. Douglas, C. H. Woo, P. M. Beaujuge and J. M. J. Fréchet, *J. Am. Chem. Soc.*, 2010, **132**, 7595–7597.
35 J. Peet, C. Soci, R. C. Coffin, T. Q. Nguyen, A. Mikhailovsky, D. Moses and G. C. Bazan, *Appl. Phys. Lett.*, 2006, **89**, 252105.
36 J. Peet, J. Y. Kim, N. E. Coates, W. L. Ma, D. Moses, A. J. Heeger and G. C. Bazan, *Nat. Mater.*, 2007, **6**, 497–500.
37 H. Choi, S.-J. Ko, T. Kim, P.-O. Morin, B. Walker, B. H. Lee, M. Leclerc, J. Y. Kim and A. J. Heeger, *Adv. Mater.*, 2015, **27**, 3318–3324.
38 T. L. Nguyen, H. Choi, S. J. Ko, M. A. Uddin, B. Walker, S. Yum, J. E. Jeong, M. H. Yun, T. J. Shin, S. Hwang, J. Y. Kim and H. Y. Woo, *Energy Environ. Sci.*, 2014, **7**, 3040–3051.
39 Y. Cui, H. Yao, J. Zhang, T. Zhang, Y. Wang, L. Hong, K. Xian, B. Xu, S. Zhang, J. Peng, Z. Wei, F. Gao and J. Hou, *Nat. Commun.*, 2019, **10**, 2515.
40 J. Yuan, Y. Zhang, L. Zhou, G. Zhang, H.-L. Yip, T.-K. Lau, X. Lu, C. Zhu, H. Peng, P. A. Johnson, M. Leclerc, Y. Cao, J. Ulanski, Y. Li and Y. Zou, *Joule*, 2019, **3**, 1140–1151.
41 N. Y. Doumon, G. Wang, X. Qiu, A. J. Minnaard, R. C. Chiechi and L. J. A. Koster, *Sci. Rep.*, 2019, **9**, 4350.
42 B. J. Tremolet de Villers, K. A. O'Hara, D. P. Ostrowski, P. H. Biddle, S. E. Shaheen, M. L. Chabinyc, D. C. Olson and N. Kopidakis, *Chem. Mater.*, 2016, **28**, 876–884.
43 A. J. Pearson, P. E. Hopkinson, E. Couderc, K. Domanski, M. Abdi-Jalebi and N. C. Greenham, *Org. Electron.*, 2016, **30**, 225–236.
44 A. Tournebize, A. Rivaton, H. Peisert and T. Chassé, *J. Phys. Chem. C*, 2015, **119**, 9142–9148.
45 H. Li, D. He, P. Mao, Y. Wei, L. Ding and J. Wang, *Adv. Energy Mater.*, 2017, **7**, 1602663.
46 R. Yu, H. Yao, L. Hong, Y. Qin, J. Zhu, Y. Cui, S. Li and J. Hou, *Nat. Commun.*, 2018, **9**, 4645.
47 R. Yu, H. Yao, Z. Chen, J. Xin, L. Hong, Y. Xu, Y. Zu, W. Ma and J. Hou, *Adv. Mater.*, 2019, **31**, 1900477.
48 Q. Guo, Y. Liu, M. Liu, H. Zhang, X. Qian, J. Yang, J. Wang, W. Xue, Q. Zhao, X. Xu, W. Ma, Z. Tang, Y. Li and Z. Bo, *Adv. Mater.*, 2020, **32**, 2003164.
49 X. Du, X. Li, H. Lin, L. Zhou, C. Zheng and S. Tao, *J. Mater. Chem. A*, 2019, **7**, 7437–7450.
50 P. Cheng, C. Yan, T.-K. Lau, J. Mai, X. Lu and X. Zhan, *Adv. Mater.*, 2016, **28**, 5822–5829.
51 C.-G. Wu, C.-H. Chiang and H.-C. Han, *J. Mater. Chem. A*, 2014, **2**, 5295–5303.
52 B. Xu, G. Sai-Anand, A.-I. Gopalan, Q. Qiao and S.-W. Kang, *Polymers*, 2018, **10**, 121.
53 B. Xu, G. Sai-Anand, G. E. Unni, H.-M. Jeong, J.-S. Kim, S.-W. Kim, J.-B. Kwon, J.-H. Bae and S.-W. Kang, *Appl. Surf. Sci.*, 2019, **484**, 825–834.
54 Q. Zhang, C. Bao, S. Cui, P. Zhong, K. Zhang, W. Zhu and Y. Liu, *J. Mater. Chem. C*, 2020, **8**, 16551–16560.
55 P. Fan, W. Sun, X. Zhang, Y. Wu, Q. Hu, Q. Zhang, J. Yu and T. P. Russell, *Adv. Funct. Mater.*, 2021, **31**, 2008699.
56 L. Liu, Y. Kan, K. Gao, J. Wang, M. Zhao, H. Chen, C. Zhao, T. Jiu, A. K. Jen and Y. Li, *Adv. Mater.*, 2020, **32**, 1907604.
57 Z. Wang, R. Zhang, M. Zhao, Z. Wang, B. Wei, X. Zhang, S. Feng, H. Cao, P. Liu, Y. Hao, H. Wang, B. Xu, S. J. Pennycook and J. Guo, *J. Mater. Chem. A*, 2018, **6**, 23773–23779.
58 S. Liu, S. Lin, P. You, C. Surya, S. P. Lau and F. Yan, *Angew. Chem., Int. Ed.*, 2017, **56**, 13717–13721.
59 B. J. Moon, Y. Oh, D. H. Shin, S. J. Kim, S. H. Lee, T.-W. Kim, M. Park and S. Bae, *Chem. Mater.*, 2016, **28**, 1481–1488.
60 M. M. Stylianakis, D. Konios, G. Kakavelakis, G. Charalambidis, E. Stratakis, A. G. Coutsolelos, E. Kymakis and S. H. Anastasiadis, *Nanoscale*, 2015, **7**, 17827–17835.
61 J. M. Lee, J. Lim, N. Lee, H. I. Park, K. E. Lee, T. Jeon, S. A. Nam, J. Kim, J. Shin and S. O. Kim, *Adv. Mater.*, 2015, **27**, 1519–1525.
62 X. Wan, G. Long, L. Huang and Y. Chen, *Adv. Mater.*, 2011, **23**, 5342–5358.
63 A. K. Geim and K. S. Novoselov, *Nat. Mater.*, 2007, **6**, 183–191.
64 K. S. Novoselov, A. K. Geim, S. V. Morozov, D. Jiang, Y. Zhang, S. V. Dubonos, I. V. Grigorieva and A. A. Firsov, *Science*, 2004, **306**, 666.
65 C. Tan, X. Cao, X.-J. Wu, Q. He, J. Yang, X. Zhang, J. Chen, W. Zhao, S. Han, G.-H. Nam, M. Sindoro and H. Zhang, *Chem. Rev.*, 2017, **117**, 6225–6331.
66 D. Jariwala, T. J. Marks and M. C. Hersam, *Nat. Mater.*, 2017, **16**, 170–181.
67 N. R. Glavin, R. Rao, V. Varshney, E. Bianco, A. Apte, A. Roy, E. Ringe and P. M. Ajayan, *Adv. Mater.*, 2020, **32**, 1904302.
68 S. Lin, S. Liu, Z. Yang, Y. Li, T. W. Ng, Z. Xu, Q. Bao, J. Hao, C.-S. Lee, C. Surya, F. Yan and S. P. Lau, *Adv. Funct. Mater.*, 2016, **26**, 864–871.
69 Y. Wang, J. Li, T. Li, J. Wang, K. Liu, Q. Jiang, J. Tang and X. Zhan, *Small*, 2019, **15**, 1903977.
70 Q. Liu, Z. Liu, X. Zhang, N. Zhang, L. Yang, S. Yin and Y. Chen, *Appl. Phys. Lett.*, 2008, **92**, 223303.
71 L. Bai, L. Sun, Y. Wang, Z. Liu, Q. Gao, H. Xiang, H. Xie and Y. Zhao, *J. Mater. Chem. A*, 2017, **5**, 8280–8286.
72 F. Bonaccorso, Z. Sun, T. Hasan and A. C. Ferrari, *Nat. Photonics*, 2010, **4**, 611–622.
73 M. Pumera and Z. Sofer, *Adv. Mater.*, 2017, **29**, 1605299.
74 S. Zhang, M. Xie, F. Li, Z. Yan, Y. Li, E. Kan, W. Liu, Z. Chen and H. Zeng, *Angew. Chem., Int. Ed.*, 2016, **55**, 1666–1669.
75 J. Cai, H. Wang, X. Zhang, W. Li, D. Li, Y. Mao, B. Du, M. Chen, Y. Zhuang, D. Liu, H.-L. Qin, Y. Zhao, J. A. Smith, R. C. Kilbride, A. J. Parnell, R. A. L. Jones, D. G. Lidzey and T. Wang, *J. Mater. Chem. A*, 2020, **8**, 4230–4238.
76 X. Zhang, J. Cai, C. Guo, D. Li, B. Du, Y. Zhuang, S. Cheng, L. Wang, D. Liu and T. Wang, *Small*, 2021, **17**, 2102558, DOI: 10.1002/smll.202102558.
77 J. Fu, S. Chen, K. Yang, S. Jung, J. Lv, L. Lan, H. Chen, D. Hu, Q. Yang, T. Duan, Z. Kan, C. Yang, K. Sun, S. Lu, Z. Xiao and Y. Li, *iScience*, 2020, **23**, 100965.
78 L. Ye, Y. Cai, C. Li, L. Zhu, J. Xu, K. Weng, K. Zhang, M. Huang, M. Zeng, T. Li, E. Zhou, S. Tan, X. Hao, Y. Yi, F. Liu, Z. Wang, X. Zhan and Y. Sun, *Energy Environ. Sci.*, 2020, **13**, 5117–5125.

79 S. Chen, J. Ye, Q. Yang, J. Oh, D. Hu, K. Yang, G. O. Odunmbaku, F. Li, Q. Yu, Z. Kan, Z. Xiao, C. Yang, S. Lu and K. Sun, *J. Mater. Chem. A*, 2021, **9**, 2857–2863.
80 J. Fu, H. Chen, P. Huang, Q. Yu, H. Tang, S. Chen, S. Jung, K. Sun, C. Yang, S. Lu, Z. Kan, Z. Xiao and G. Li, *Nano Energy*, 2021, **84**, 105862.
81 Y. Yan, Y. Liu, J. Zhang, Q. Zhang and Y. Han, *J. Mater. Chem. C*, 2021, **9**, 3835–3845.
82 S. Bao, H. Yang, H. Fan, J. Zhang, Z. Wei, C. Cui and Y. Li, *Adv. Mater.*, 2021, 2105301, DOI: 10.1002/adma.202105301.
83 T. Plötzing, T. Winzer, E. Malic, D. Neumaier, A. Knorr and H. Kurz, *Nano Lett.*, 2014, **14**, 5371–5375.
84 X. Zhu, *Acc. Chem. Res.*, 2013, **46**, 1239–1241.
85 Y. Yan, R. W. Crisp, J. Gu, B. D. Chernomordik, G. F. Pach, A. R. Marshall, J. A. Turner and M. C. Beard, *Nat. Energy*, 2017, **2**, 17052.